Gravitational wet avalanche pressure on pylon-like structures

B. Sovilla, Thierry Faug, A. Köhler, D. Baroudi, J.T. Fischer, Emmanuel Thibert

Cold Regions Science and Technology 126 (2016) 66–75

Contents lists available at ScienceDirect

Cold Regions Science and Technology

journal homepage: www.elsevier.com/locate/coldregions

Gravitational wet avalanche pressure on pylon-like structures

Betty Sovilla[a,*], Thierry Faug[b], Anselm Köhler[a], Djebar Baroudi[c], Jan-Thomas Fischer[d], Emmanuel Thibert[b]

[a] WSL Institute for Snow and Avalanche Research SLF, Davos, Switzerland
[b] Université Grenoble Alpes, Irstea, St-Martin-d'Héres, France
[c] Aalto University, School of Engineering, Department of Civil Engineering, Finland
[d] Austrian Research center for Forests (BFW), Innsbruck, Austria

ARTICLE INFO

Article history:
Received 8 October 2015
Received in revised form 9 February 2016
Accepted 8 March 2016
Available online 19 March 2016

Keywords:
Wet avalanches
Avalanche pressure
Gravitational pressure
Granular flow

ABSTRACT

Low-speed wet avalanches exert hydrostatic forces on structures that are flow-depth dependent. However, the pressure amplification experienced by smaller structures has not been quantified previously. In particular, recent wet avalanche pressure measurements, performed with small cells at the "Vallée de la Sionne" test site, indicate significantly higher pressures than those considered by engineering guidelines and common practice rules based only on the contribution of inertial forces. In order to gain a deeper understanding and investigate the relevance of these measurements for structural design, we analyzed data measured on obstacles of different shapes and dimensions. The pressure measured on a 1m^2 pressure plate was, on average, 1.8 times smaller than the pressure measured on a 0.008m^2 piezoelectric cell installed on a 0.60 m wide pylon and 2.9 times smaller than the pressure measured on a 0.0125m^2 cantilever sensor extending freely into the avalanche flow. Further, avalanches characterized by a gravitational flow regime exerted pressures that increased linearly with avalanche depth. For Froude numbers larger than 1, an additional square-velocity dependent contribution could not be neglected. The pressure variations encountered by the different obstacles could be explained quantitatively with a granular force model, that assumes the formation of a mobilized volume of snow granules extending from the obstacle upstream whose dimensions depend on the incoming flow depth and the obstacle width. This mobilized volume is associated with the formation of a network of gravity-loaded grain-grain contacts, also called granular force chains, which densifies in front of the obstacle, producing force amplification. Our results underscore the fundamental influence of the dimensions of both the sensor and the obstacle on pressures in the gravitational flow regime and may help to improve rules for structural design.

1. Introduction

The calculation of pressure exerted by gravitational mass flows on structures of different dimensions and shapes is a long-standing issue that is not yet resolved (Ancey and Bain, 2015; Gauer et al., 2008).

In literature, the pressure exerted on obstacles is calculated by considering a contribution from a fast impact, that is proportional to the square of velocity (inertial term) and a contribution from a slow thrust of material around the obstacles that is proportional to the flow depth, similar to a hydrostatic contribution (gravitational term) (Salm, 1966; Savage and Hutter, 1991; Voellmy, 1955). The flow regimes associated with these contributions are frequently defined as inertial and gravitational, respectively (Ancey and Bain, 2015; Faug, 2015).

Normally, the Froude number is used as a criterion to distinguish between the two contributions, with $Fr \gg 1$ associated with the inertial regime and $Fr \ll 1$ with the gravitational regime. For intermediate Froude numbers, the avalanche pressure can not be expressed as a simple function of either avalanche velocity or flow depth, and the flow regime is defined as transitional. For granular flows, Faug (2015) found that the transitional regime covers a wide range of Froude numbers, from 0.1 to 10. Dense granular avalanches typically have Froude numbers within this range, which suggests that they may belong to the transitional regime.

This result indicates that the transitional regime is not simply defined by $Fr = 1$, the value that traditionally emerges from dimensional analysis of inviscid flows in conventional fluid mechanics. For frictional granular flows, such as snow avalanches, other

* Corresponding author at: WSL Institute for Snow and Avalanche Research SLF, Flüelastrasse 11, 7260, Davos Dorf, Switzerland.

http://dx.doi.org/10.1016/j.coldregions.2016.03.002

dimensionless numbers are needed. $Fr = 1$ is not a relevant critical value for at least two reasons. First, it is quite well established that the Coulomb number (Ancey and Evesque, 2000) or the inertial number (Forterre and Pouliquen, 2008) that is the square root of the Coulomb number, are more suitable dimensionless numbers for a certain range of granular flow conditions. When shear is concentrated at the base of the flow, as in many snow avalanches (Kern et al., 2009), the macroscopic inertial number may be proportional to the Froude number (Ancey and Bain, 2015) but is not equal to the Froude number. Second, considering the finite width of the avalanche flow leads to another expression of the Froude number (a function of flow rate, flow cross section and width of the free surface), and thus to another transitional value of the Froude number. These problems regarding the dimensionless numbers, fully relevant to snow avalanches, are currently unresolved. However, the knowledge of both the thickness and the velocity of the avalanche flow are sufficient to determine the value of the infinite-wetted-section Froude number, which provides a rough yet quick indication of the range of the flow regime (gravitational, transitional, or inertial).

In snow avalanche engineering, the pressure contribution from the gravitational term is normally not considered (Rudolf-Miklau et al., 2015; Jóhannesson et al., 2009), although recommendations to include it in pressure calculations do exist (see Chapter 4 in Ancey (2006) and references therein). In snow avalanche science, the pressure contribution from the gravitational term is usually considered small or even negligible in comparison to the contribution from the inertial term. However, recent full-scale measurements on wet avalanches performed at the "Vallée de la Sionne" (VdlS) test site (Sovilla et al., 2010), and back analysis of avalanche damaging infrastructures (Ancey and Bain, 2015) have shown clearly that avalanches moving in a gravitational flow regime can also exert very large impact pressures, thus potentially becoming relevant for the design of infrastructures. Further, no clear definition of the transition regime exists in snow avalanche science, and thus there is no relationship with which to calculate impact pressure for avalanches characterized by Froude numbers in the range 0.1–10, where inertial and gravity-driven forces have the same order of magnitude.

At the VdlS, impact pressures are measured on sensors mounted on finite-size obstacles, which resemble ski or chairlift pylons (Sovilla et al., 2008a). Sensors have various dimensions, with areas varying between 0.008 and 1m^2 (Schaer and Issler, 2001; Sovilla et al., 2008b). Finite-sized obstacles, also known as narrow obstacles, are normally defined as structures with a width on the same scale or smaller than the flow depth (Jóhannesson et al., 2009). For such obstacles, the flow is not laterally confined and diverted around the obstacle rather than passing over the obstacle.

Sovilla et al. (2010) reported impact pressures exerted by wet avalanches, in the gravitational flow regime (Froude numbers typically smaller than 1, even if such a critical value still spurs debate, as discussed previously), that were measured with piezoelectric load cells 0.10 m in diameter, the smallest sensors at the site (Fig. 1). As a follow-up study to that preliminary analysis, Baroudi et al. (2011) compared these data to measurements performed, at the same location, using rectangular cantilever sensing devices of a slightly larger area of 0.0125m^2. These studies demonstrated a strong dependency of pressure measurements on sensor geometry and flow regimes, specifically for wet avalanches.

In particular, the properties of the snow entrained by an avalanche during its motion (density, temperature) significantly affect flowdynamics and can determine whether the flowing material forms granules or maintains its original fine-grained morphology. In general, a cold and light snow cover can be brought into suspension easily, while warmer and more cohesive snow may form a granular, denser layer. This diversification has a fundamental influence not only on the mobility of the flow but also on the impact pressure avalanches exert on structures (Sovilla et al., 2015). Steinkogler et al. (2015) recently

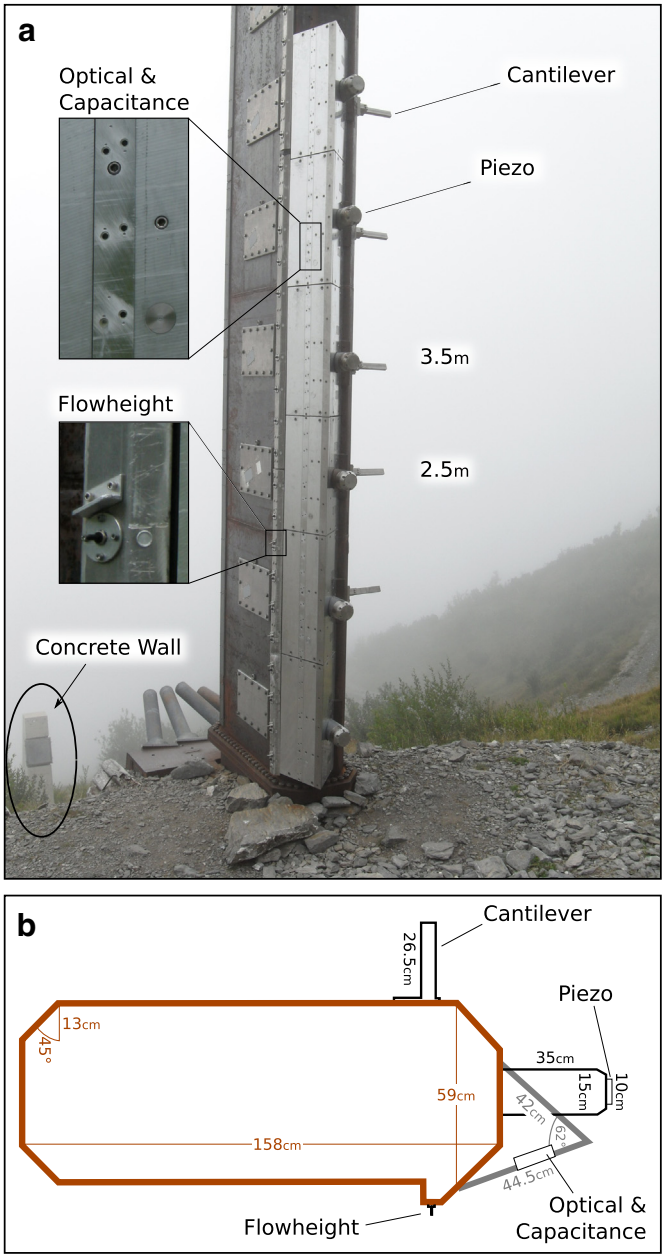

Fig. 1. The 20 m high VdlS instrumented pylon. Panel *a* shows an overview with the piezo and cantilever impact sensors and close-up of optical sensors, capacitance probes and flow height sensors. Panel *b* shows a cross section of the pylon with the geometrical details of the sensor installation.

showed that granulation in snow occurred when the snow temperature exceeded −1 ° C. Different snow conditions result in different granulation regimes. Specifically, granules can be differentiated into moist or wet, depending on the liquid water content of snow, showing significantly different mechanical properties upon collision. Thus, granulation is mostly relevant for snow with a temperature higher than −1 ° C and therefore it plays a crucial role for avalanches close to the melting point. The avalanches studied in this paper are all in this category, and their characteristic flow regime is easily identifiable by the plug-like behavior measured at the pylon (Sovilla et al., 2008a); thus, they are expected to behave as granular flows. Nevertheless, we do not have information concerning the snow liquid water content or the exact temperature of the snow in the area of the obstacles, since appropriate measuring devices are not available at the site,

and thus a precise distinction between different granulation regimes is not possible.

The conclusion drawn from previous analysis(Sovilla et al., 2010) cannot simply be extrapolated to finite-sized obstacles that are relevant for engineering purposes, such as ski or chairlift pylons. In particular, large pressures measured with small cells may be related to the dimensions of the sensors, since they are of a similar size as the granules (10–25 cm in diameter) that usually characterize wet flows (Steinkogler et al., 2015).

In order to investigate whether high pressures measured with small sensors also occur at larger scale, i.e. the scale of real structures impacted by avalanches, we compared pressures measured in wet, granular avalanches with sensors of different dimensions. On this basis, we determined a reduction coefficient from small to large obstacles.

Additionally, we compared measurements with a theoretical model recently proposed by Faug (2015) to describe granular flow interaction with obstacles. This model assumes that, in a mobilized volume whose geometry depends on both structure width and avalanche flow depth, gravity-loaded grain-grain contacts are likely to form. The model quantifies an amplification factor explaining how these contacts enhance the force undergone by the obstacle.

2. Methods

2.1. Infrastructure and sensors

Pressure measurements are performed on an oval-shaped steel pylon, 20 m high, 0.59 m wide and 1.58 m long (Fig. 1). Six piezoelectric load cells, hereafter designated as piezo sensors, are installed on the uphill face of the pylon, with 1 m vertical spacing, from 0.5 to 5.5 m above ground. The sampling frequency is 7.5 kHz and they have a diameter of 0.10 m with an area of 0.008m^2. Geometrical details of the sensor installation are shown in Fig. 1b.

The cantilever sensing devices are installed on the right side of the pylon, at the same height as the piezoelectric sensors, and extend into the avalanche flow (Fig. 1b). They have an area of about 0.0125m^2 and an acquisition frequency of 2.0 kHz (Baroudi et al., 2011).

The pylon is also equipped with optical sensors for the determination of velocity profiles (between 0.5 and 6 m above ground) (Dent et al., 1998; Tiefenbacher and Kern, 2004), capacitance probes for density measurements (at 3 and 6.5 m) (Louge et al., 1997) and flow depth sensors (toggles switches between 0.25 and 7.5 m).

Thirty meters downstream from the pylon a small concrete wall, 1 m wide, 4.5 m high and 3.5 m long, supports a 1m^2 pressure plate (bottom left in Fig. 1), which is mounted with its center at a height of 3 m above ground surface (Fig. 2). The pressure plate is supported by four strain-gauged pins. The set-up makes it possible to measure normal and shear forces along the horizontal and vertical directions with a sampling frequency of 2 kHz. A more detailed description of the infrastructure and sensors can be found in Sovilla et al. (2008b) and Schaer and Issler (2001).

2.2. Criteria for data comparison

The pylon and the plate are approximately 30 m apart; thus, it is very important to verify that the avalanche reached both infrastructures with similar velocities and depths. As a general criterion, we observe deposition patterns, and avalanche dynamics from pictures and videos to visually identify avalanches that have interacted with both infrastructures in a similar manner. Avalanches characterized by a large width in the run-out zone are better suited for the analysis since they exert a similar pressure over a large area. Only signals comparable in duration and shape were included in the analysis presented here.

Given that the 1m^2 plate is mounted with its center 3 m above the ground and vertically extends from 2.5 to 3.5 m, we compared these data with the average impact pressure measured with the small sensors on the pylon, 2.5 m and 3.5 m above ground. This implies that the sliding surface is the same at the plate and pylon locations. Further, velocity and flow depth measurements are performed only at the pylon, and thus the pressure data at the plate need to be coupled with measurements taken 30 m away. To account for the time shift between pylon and wall measurements, we moved the time origin of the two records using the avalanche front velocity.

Pressure is strongly correlated with the flow regime, with gravitational, transitional and inertial regimes characterized by completely different obstacle–avalanche interactions (Baroudi et al., 2011; Sovilla et al., 2008a). Thus, data need to be classified into these categories. Difficulties arise when many flow regimes are present in one single avalanche. We used different criteria to associate flow regimes to impact signals, including: (1) analyzing the ratio between pressure fluctuations and average pressure, which is very different for each flow regime (Sovilla et al., 2010) and (2) comparing the velocity profiles and their fluctuations to distinguish between plug flow, sheared flow and more energetic zones of the signal (Sovilla et al., 2015; Steinkogler et al., 2015). In the analysis presented here, only data pertaining to the gravitational and transition regimes were considered. In other words, we manually excluded time slots for which inertial forces prevail.

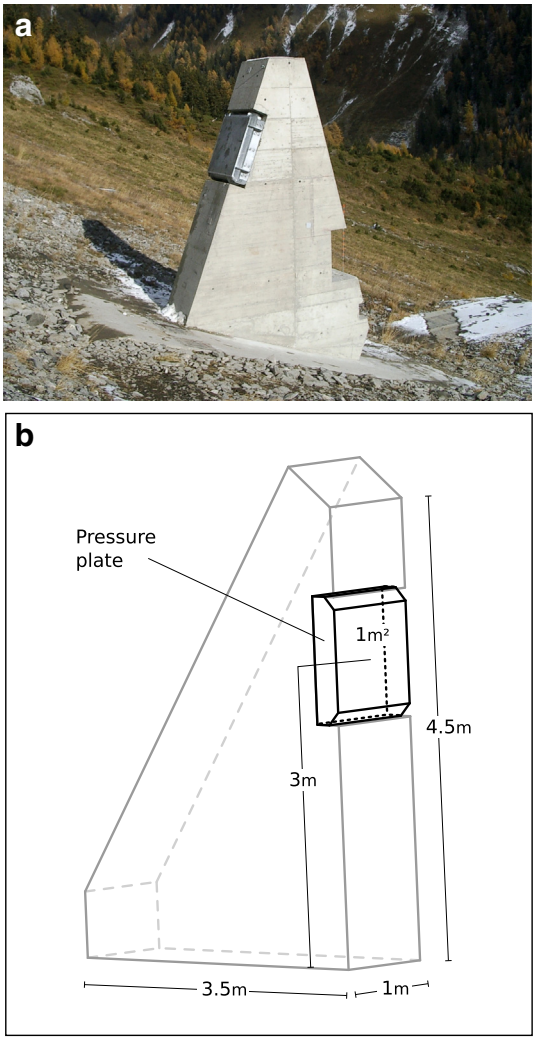

Fig. 2. The small concrete wall supports a 1m^2 pressure plate. The plate is mounted with its center at a height of 3 m above the ground surface.

Table 1
Overview of avalanches used in this analysis. The parameters neglect information referring to the inertial flow regime, when present.

Date	Av. #	$v(ms^{-1})$	H_{max} (m)	Fr
01-03-2007	8448	1–3	4	$Fr < 1$
30-12-2009	20103003	6–10	6–7	$1 \leq Fr \leq 2$
06-12-2010	20113003	1–2	2.5	$Fr < 1$
01-02-2013	20133019	1–5	3.5	$Fr \leq 1$
02-02-2013	20133021	2–7	5	$Fr < 1.5$

3. Data

Measurements at both the plate and the pylon have been performed since the winter season 2004/05. Over this period, we have recorded impact pressures of about 40 avalanches, of varying dimension and typology, that interacted with both infrastructures. Five of these were wet avalanches and were analyzed in this study. All wet avalanches released naturally, making it difficult to establish the exact location of release and the avalanche volumes. Nevertheless, pictures taken after the avalanche release allowed us to characterize their dimensions in the avalanche deposition zone, i.e. at the location of the measurements. Table 1 shows the most relevant avalanche parameters characterizing the flow, namely the avalanche velocity, v, the maximum avalanche depth, H_{max} and the Froude number, Fr. It is noteworthy that our analysis distinguished between the flow depth, H, which is the total avalanche flow depth with respect to the avalanche sliding surface, and the effective flow depth, H_{eff}, which is the avalanche flow depth with respect to the position of the sensor where the pressure is measured, z_s. The effective flow depth is calculated as: $H_{eff} = H - z_s$.

3.1. Avalanche #8448

Avalanche #8448 released naturally on 1 March 2007 at 21:19. It released after a snow precipitation event of nearly 0.4 m on an existing 2–3 m thick snowpack, according to measurements made close to the release zone at an altitude of 2390 m.a.s.l. Air temperature was about −4 ° C in the release zone and slightly above 0 ° C in the run-out zone. The avalanche started as a dry flow but developed into a typical wet, dense, slow flow, at lower altitude. At the pylon, the avalanche had an average velocity of 1–3 ms^{-1} and was characterized by plug flow (Kern et al., 2009), with a sliding surface approximately 2.0 m above ground. At the same location, the maximum flow depth was about 4.0 m (Fig. 3, left). From permittivity measurements performed 3 m above ground, we estimated the flow density to be 400kg m^{-3} (Louge et al., 1997). The avalanche was characterized by a gravitational flow regime (Sovilla et al., 2010).

Signals from the piezo and plate sensors were largely consistent except for the first five seconds of the measurements, where the pressure at the plate showed a decreasing trend but the pressure at the pylon showed the opposite (increasing) trend (Fig. 3, right). For this reason, the beginning of the signal was excluded from the analysis (dashed area in Fig. 3). On the contrary, a large part of the signal from the cantilever sensor showed a different trend (gray line in Fig. 3). This difference was interpreted as large fluctuations occurring during the loading of the most energetic part of the avalanche (Baroudi et al., 2011). This part of the measurements was not considered for this study. Further informations on this avalanche can be found in Kern et al. (2009), Sovilla et al. (2010) and Baroudi et al. (2011).

3.2. Avalanche #20103003

Avalanche #20103003 released naturally on 30 December 2009 at 13:30. At the time of release, about 0.20 m of new snow had fallen in the preceding 24 h on a snow cover of 1.80 m, as measured close to the release zone at an altitude of 2390 m.a.s.l. Air temperature was −4 ° C in the release zone, and around 0 ° C in the run-out zone. These values indicate that the snow precipitation might have evolved into rain at lower altitude. The avalanche started as a dry flow but at the pylon was characterized by a dilute, fast moving front, followed by a denser, slower avalanche body moving with velocities up to approximately 10 ms^{-1}. Oscillations in velocity and flow depth indicate that the flow was characterized by successive surges. This large avalanche had a maximum flow depths of up to 6–7 m at the pylon and it slid directly on the rock ground (Fig. 4, left).

Signals from the different sensors were largely consistent, except during the first part of the measurements where the pressure at the plate showed a decreasing trend whereas an increasing trend was observed at the pylon (Fig. 4, right). For this reason, the first ten seconds of signal were excluded from the analysis (dashed area in Fig. 4).

Apart from the dilute frontal part, this avalanche had $1 \leq Fr \leq 2$. Thus, it was largely characterized by a transition flow regime where gravitational forces were balanced by inertial forces. Further information on this avalanche can be found in Kogelnig et al. (2011).

3.3. Avalanche #20113003

Event #20113003 occurred on 6 December 2010 at 18:30. The avalanche naturally released after a snow precipitation event of about 0.50 m in the preceding 48 h on a snow cover of 0.80 m, as measured close to the release zone at an altitude of 2390 m a.s.l. Air temperature in the release zone was −4 ° C. The motion of the avalanche could be observed using a new phased array FMCW radar system (GEODAR) (Vriend et al., 2013). At the pylon, the avalanche was characterized by three distinct surges. The first two surges were dry diluted and traveled at a maximum velocity of 24ms^{-1} and 21ms^{-1}, respectively. The third surge traveled slowly at 1–2 ms^{-1}, had the typical characteristics of a wet dense flow with a maximum flow depth of 2.5 m, and was characterized by a $Fr<1$, and thus by a gravitational regime. Density measurements of this avalanche have been presented by Sovilla et al. (2015). The sliding surface of this avalanche was estimated to be 1.2 m above ground.

3.4. Avalanche #20133019

Event #20133019 naturally released on 1 February 2013 at 17:16 after a snow precipitation event of about 0.35 m in the preceding 36 h on a snow cover of 2.2 m, as measured close to the release zone at an altitude of 2390 m a.s.l.. Air temperature in the release zone was −2.5 ° C. The GEODAR data confirms that, at the pylon, the avalanche had mostly a wet flow behavior characterized by velocity in the range 1–5ms^{-1}. A small powder component was probably still present at this distance but rapidly disappeared. The deposit depicted the typical characteristics of wet avalanche debris with granules aggregations. At the pylon location, the avalanche slid on a 1 m thick previous snow deposit and was characterized by plug flow. Maximum flow depth was about 3.5 m. The avalanche was characterized by a gravitational regime.

3.5. Avalanche #20133021

Event #20133021 naturally released on 2 February 2013 at 05:28 after a snow precipitation event of about 0.70 m in the preceding 42 h on a snow cover of 2.2 m, according to measurements made close to the release zone at an altitude of 2390 m a.s.l.. Air temperature in the release zone was −4.7 ° C. The GEODAR data confirms that the avalanche was traveling slowly at the pylon and had the typical characteristics of a wet flow avalanche, with velocities in the range 2–7 ms^{-1}. A small powder component was probably still present

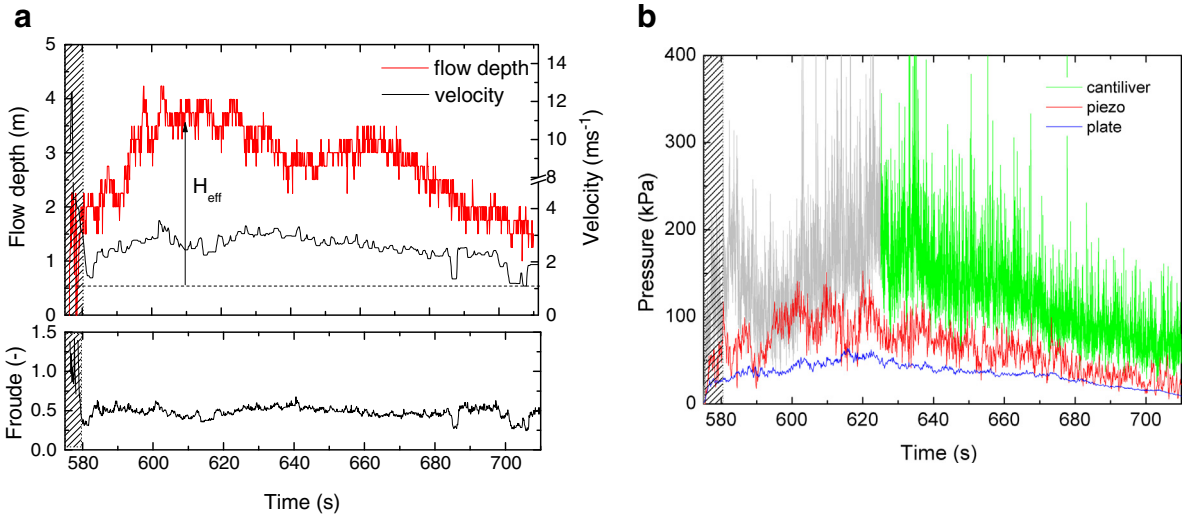

Fig. 3. Avalanche #8448. The top left panel shows flow depth, H, and velocity at 3 m above ground, while the bottom left panel shows the corresponding Froude numbers. The horizontal dashed line in the upper left panel highlights the position of the impact pressure measurements, which was used to define the effective flow depth, H_{eff}. The right panel shows the impact pressures measured with the plate (blue), piezo (red) and cantilever (green) sensors. The dashed area and the gray data highlight measurements excluded from the analysis. (For interpretation of the references to color in this figure legend, the reader is referred to the web version of this article.)

at this distance but rapidly disappeared. The deposit depicted the typical characteristics of wet avalanche debris. At the pylon, the avalanche was characterized by plug flow with a small shear rate, and it slid on an old deposit about 1.0 m thick and reached a maximum flow depth of about 5 m. The avalanche was characterized by a Froude number in the range 0.6–1.5; thus, it had characteristics of both the gravitational and transition regimes.

4. Snow avalanche pressure in the gravitational and transitional regimes

Recently, Sovilla et al. (2010) provided further evidence that the impact pressure of wet avalanches, characterized by a gravitational regime, increases proportionally to the flowing depth according to:

$$p = \zeta \rho g H_{eff}, \tag{1}$$

where H_{eff} is the location of the pressure measurement in respect to the avalanche surface, ρ is the flow bulk density, g is the gravitational acceleration and ζ is an empirical parameter. Adopting $\rho = 400 \pm 80 \text{kg m}^{-3}$, as derived from permittivity measurements (Louge et al., 1997), Eq. (1) was fitted to representative vertical pressure profiles using ζ values in the range 7.2–8.1. Furthermore, Eq. (1) is found to match results from a number of laboratory experiments on the force experienced by solid objects in low-speed granular flows (see for instance Albert et al. (1999) and Wieghardt (1975)).

Following the study of Sovilla et al. (2010), in order to understand how sensor and obstacle dimensions influence pressure measurements, this fitting was extended to other measurements. Fig. 5 shows, as an example, the fitting of Eq. (1) for avalanche #8448 in the time domain. Specifically, Eq. (1) was fitted to the pressure signals of piezo (red line), plate (blue line) and cantilever (green line) data by properly adapting the parameter ζ and considering the effective flow depth, H_{eff}. In particular, ζ was solved with a linear least-squares regression of the pressure and flow height data. The

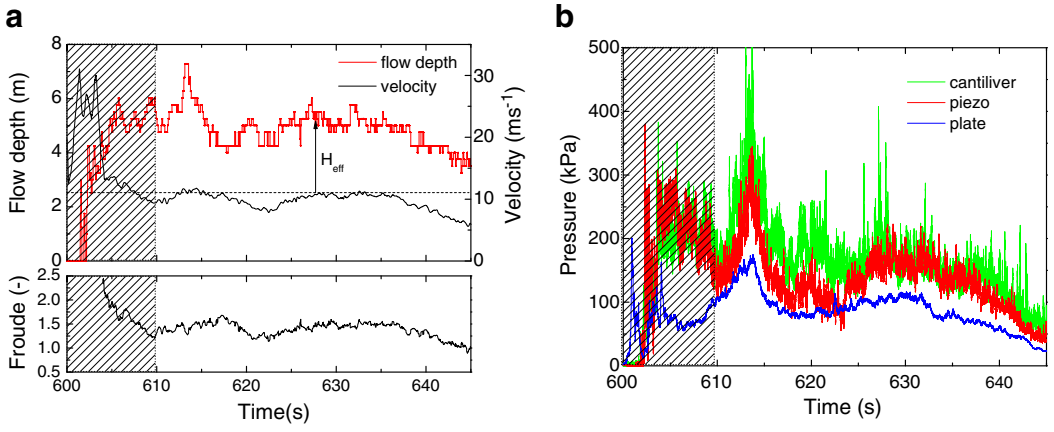

Fig. 4. Avalanche #20103003. The top left panel shows flow depth, H_{eff}, and velocity at 3 m above ground, while the bottom left panel shows the corresponding Froude numbers. The horizontal dashed line in the upper left panel highlights the position of the impact pressure measurements, and it is used to define the effective flow depth, H_{eff}. The right panel shows the impact pressures measured with the plate (blue), piezo (red) and cantilever (green) sensors. The dashed area highlights measurements excluded from the analysis. (For interpretation of the references to color in this figure legend, the reader is referred to the web version of this article.)

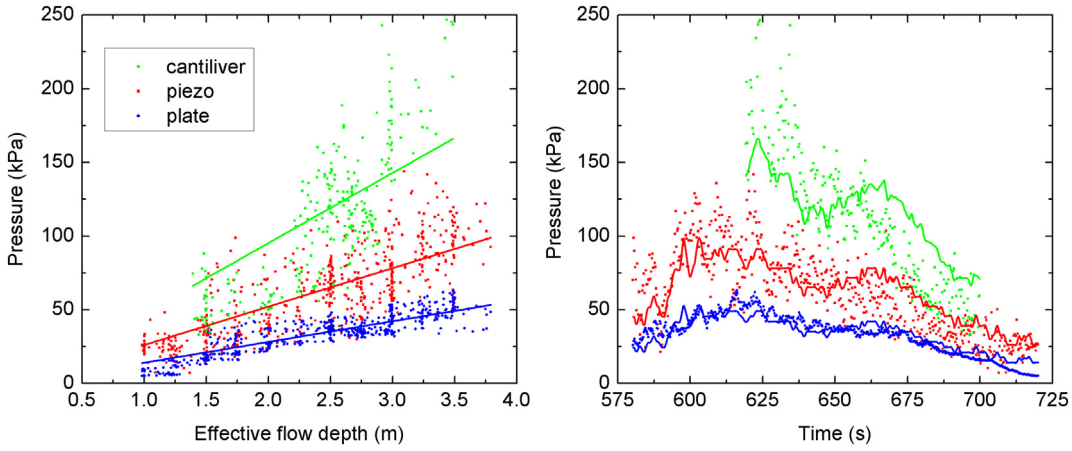

Fig. 5. Impact pressure as a function of effective flow depth, H_{eff}, (left panel) and as a function of time (right panel) for avalanche #8448. Dots indicate measurements performed with piezo (red), plate (blue) and cantilever (green) sensors. Continuous lines show best fits for the Eq. $p = \zeta \rho g H_{eff}$ using $\zeta = 6.5 \pm 1.4$, 3.7 ± 0.5 and 12.1 ± 3.0 for piezo, plate and cantilever measurements, respectively. (For interpretation of the references to color in this figure legend, the reader is referred to the web version of this article.)

confidence interval for ζ is the standard deviation between the fit and the data.

An exception to the linear fitting is represented by avalanche #20103003, which was characterized by a Froude number between 1 and 2 and maximum velocities above 10ms^{-1}, and thus, characterized by a transitional flow regime. In this case, the gravitational component alone could not satisfactorily reproduce the load and an additional inertial contribution needed to be considered. In a first approximation, the total load for avalanche #20103003 was calculated as:

$$p = \frac{1}{2} C_d \rho v^2 + \zeta \rho g H_{eff}, \tag{2}$$

where v is the velocity of the flow upstream the obstacle and C_d is a drag coefficient, which normally depends on the form and size of the object, but is also a function of the flow regimes and thus depends on dimensionless numbers such as the Reynolds, *Re*, and Froude, *Fr*, numbers.

The drag coefficient is normally chosen following the criteria defined by standard pressure calculations in the inertial flow regime (Rudolf-Miklau et al., 2015; Jóhannesson et al., 2009; Salm et al., 1990).

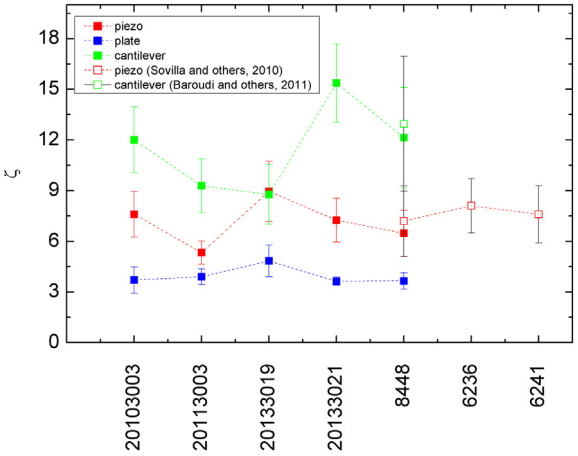

Fig. 6. Best fit coefficient ζ for all avalanches in Table 1 using Eq. (1). Green squares represent cantilever sensors, red squares piezo sensors and blue squares the plate. Red open squares represent ζ values obtained by a similar analysis in Sovilla et al. (2010). (For interpretation of the references to color in this figure legend, the reader is referred to the web version of this article.)

It is noteworthy that these values are normally valid for calculations where only inertial contributions are considered. This implies that, in cases where the gravitational term is dominant, these coefficients need to be considered as an approximation. Following the rules defined in Salm et al. (1990), Jóhannesson et al. (2009), and Rudolf-Miklau et al. (2015), we selected a $C_d = 3$, which corresponds to a round cylinder hit by a wet flow avalanche.

Fig 6 shows the best fit coefficients ζ for the examined avalanches, with blue dots representing measurements performed at the large plate, red dots representing measurements performed with the piezo sensors and green dots representing measurements performed with the cantilever sensors. The plot also includes the ζ coefficients found by Sovilla et al. (2010) by analyzing impact pressures from piezo sensors of three wet avalanches. Sovilla et al. (2010) estimated $\zeta = 7.2 \pm 2.1, 8.1 \pm 1.6$ and 7.6 ± 1.7, for avalanches #8448, #6236 and #6241, respectively, using a linear fitting applied to a representative vertical pressure profile.

Fig. 6 shows that, on average, the parameter ζ strongly varies between sensors, indicating a dependency of ζ on the dimensions either of the measurement device or of the structure on which the sensor is installed. Further variability in ζ is observed among measurements performed with the same sensor, indicating the influence of the intrinsic material properties, such as liquid water content or granulometry (Steinkogler et al., 2015).

Finally, Fig. 7 shows the coefficient $\zeta(t)$, calculated as the ratio between the impact pressure from the piezo (red line) and plate (blue line) sensors for avalanche #8448, $p(t)$, scaled by the gravitational pressure contribution $\rho g H_{eff}(t)$. $\zeta(t)$ is compared with the constant, best fit coefficient ζ (orange lines) and the effective flow depth, $H_{eff}(t)$ (black lines). We observed that a constant ζ reproduced measurements fairly well for most of the signal but the quality of the matching decreased for the smaller flow depths, suggesting the coefficient ζ may also have an intrinsic flow depth dependence.

5. Pressure on a thin structure from a mobilized volume of particle

The nature of the pressure exerted by a slow thrust of snow on a thin obstacle is not fully understood. Nevertheless, it is generally assumed that the cause of such a pressure is connected with the formation of a mobilized volume of grains that are disturbed by the presence of the obstacle (Faug, 2015; Sovilla et al., 2010) or by the formation of a dead zone upstream of the obstacles or sensor (Baroudi et al., 2011).

Recent numerical simulations on a thin object dragged into a granular medium have demonstrated the existence of a network of force chains extending from the intruder into the granular material flowing around it (Tordesillas et al., 2014). This network, or mobilized volume, is rather circular and much denser ahead of the intruder (Tordesillas et al., 2014). By analogy, we expected a denser force chains network of snow granules to form upstream the obstacles in VdlS.

Assuming the pressure on the obstacle is defined by the mobilized volume, this force is likely to depend on the obstacle dimensions as suggested by Fig. 6, but also on the depth of the incoming flow, as suggested by Fig. 7. We discuss hereinafter how a recent model carefully calibrated using a great number of force data for granular flows around thin objects (Faug, 2015) may be able to account for those effects.

Faug (2015) presented a new semi-empirical model that describes the total force exerted by the particle flow on the obstacle as a function of the width of the structure, D, and the depth of the incoming flow, H:

$$F = \frac{\pi}{8}\rho g H(\omega D + \psi H)^2 (\sin\theta - \mu_e \cos\theta), \quad (3)$$

where θ is the slope angle, μ_e is the effective friction of the granular material, and ω and ψ are parameters that describe the increase in the mobilized volume with the obstacle width and the flow height, respectively. It is assumed that the mobilized volume, V, has a cylindrical form, extending across the entire immersed height of the obstacle, and satisfies $V = HS$, where S is the typical surface of the mobilized volume surrounding the obstacle. It is worth noting that the effective friction μ_e is, by construction, smaller than θ in Eq. (3). Note also that, Eq. (3) is only valid for $D \geq d$, and $H > nd$ where d is the particle diameter and n = 5–10. Below this limit, a continuum approach is not reasonable for granular materials.

Faug (2015) found that the diameter D^* of the circular surface S could be described by a linear dependency with obstacle width and incoming flow depth in the form: $D^* = \omega D + \psi H$. The pre-factor $(\sin\theta - \mu_e cos\theta)$ in Eq. (3) indicates that the force contribution from the mobilized volume is nothing more than its apparent weight, i.e. the weight of the mobilized volume decreased by the effective friction force.

The parameters ω and ψ were found to vary in relatively narrow ranges for data from granular flows (Faug, 2015): $\omega = 2$–6 (mean value around 3) and $\psi = 0.5$–2.4 (mean value around 1.5). It is worth stressing that the parameters ω and ψ are, by construction, associated with the hypothetical geometry of the mobilized volume, i.e. a cylinder of height H. Faug (2015) assumed that this relationship is reasonable for granular flows, in light of the discrete numerical simulations on a small intruder dragged onto a granular medium by Tordesillas et al. (2014). This model has been applied to the measurements performed with the piezo and plate, which can be easily extended to represent the load exerted on thin objects, i.e. the pylon and the wall. In particular, for the piezo measurements, we assumed the volume mobilized upstream of the pylon was controlled by the pylon geometry and thus dependent on the pylon width, $D = 0.60$ m, rather than on the sensor diameter, $D = 0.10$ m. For this reason, in the following calculations the piezo measurements were associated with $D = 0.60$ m, corresponding to the pylon width. The cantilever sensors were not considered in this analysis, as they extended into the flow as individual arms (Fig. 1,b).

To compare our data with the model of Faug (2015), Eq. (3) needs to be matched with Eq. (1). This can only be done if the modeled amplification factor ζ_m obeys the following relationship:

$$\zeta_m(t) = \frac{\pi}{4}\left(2\omega\psi + \psi^2\frac{H(t)}{D} + \omega^2\frac{D}{H(t)}\right)(\sin\theta - \mu_e\cos\theta). \quad (4)$$

Again, this equation is only valid for $D \geq d$, and $H > nd$, where d is the particle diameter and n = 5–10. Before providing detailed results of calculations, it is interesting to analyze the qualitative trends predicted by Eq. (4) for values of H/D much higher than 1, as in our case. First, a similar granular flow (H kept constant) impacting two thin obstacles of distinct widths is likely to exert a greater pressure (largest ζ_m) on the obstacle whose width D is the smallest. This outcome from Eq. (4), if applied to full-scale wet snow avalanches, is consistent with Fig. 6, which shows larger pressures for the pylon ($D = 0.6$ m) than for the plate ($D = 1$ m). Second, Eq. (4) suggests that a decrease in H/D leads to a decrease in ζ_m. Fig. 7 shows this trend at the tail of the wet avalanche (after $t = 670$ s): ζ_m does not remain constant but is significantly reduced while the avalanche depth decreases.

As an example, we apply this model to avalanche #8448. We consider $\theta = 21°$, corresponding the local slope at the locations of the obstacles, and a constant density of 400kg m^{-3}. For snow, the effective friction μ_e may vary a lot depending on the type of snow and the frictional boundary conditions at the sliding surface. Since this experimental information was not available, it is reasonable to assume that the slope on which the avalanche stopped (15°) can provide a rough estimation of the effective friction $\mu_e = tan15° = 0.27$. Note that $\mu_e = 0.27$ is compatible with the typical values of effective friction found for full-scale wet snow avalanches by Naaim et al. (2013).

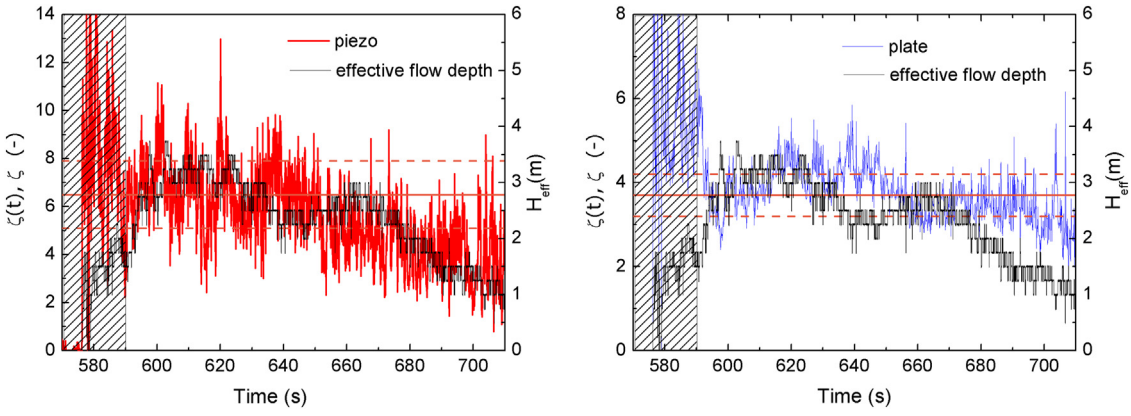

Fig. 7. Coefficients $\zeta(t)$ and ζ for avalanche #8448. $\zeta(t)$ was calculated as the avalanche pressure $p(t)$ scaled by the gravitational pressure contribution $\rho g H_{eff}(t)$. The left panel shows the data from the piezo sensor (red line) while the right panel shows the data from the plate (blue line). The orange horizontal lines show the best fit ζ coefficients and standard deviations (6.5 ± 1.4 and 3.7 ± 0.5 for piezo and plate sensors, respectively). Black lines show the effective avalanche depth, H_{eff}. The dashed area highlights data not used in the analysis. (For interpretation of the references to color in this figure legend, the reader is referred to the web version of this article.)

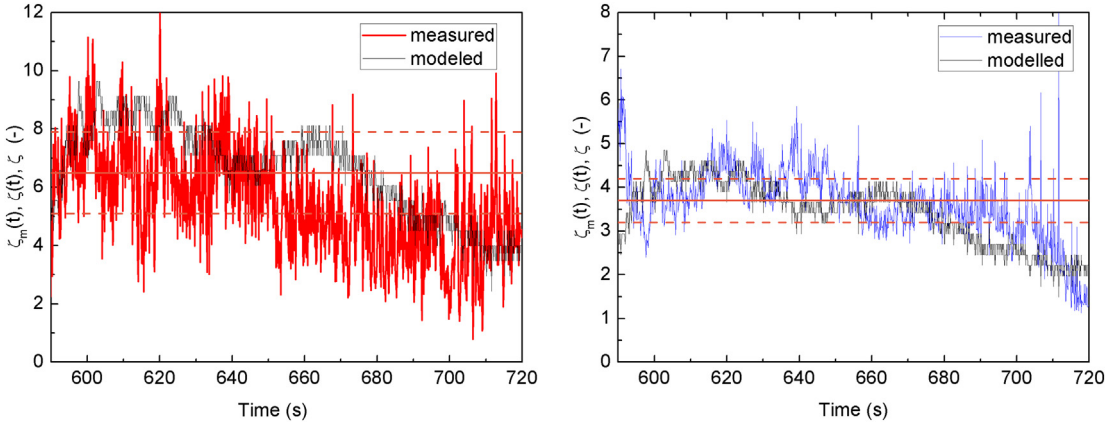

Fig. 8. Coefficients $\zeta_m(t)$, $\zeta(t)$ and ζ for avalanche #8448. The panels shows $\zeta(t)$ values derived from measurements, using $\zeta(t) = p(t)/(\rho g H_{eff}(t))$, for the piezo sensor (left, red line) and for the plate sensors (right, blue line). Black lines show the parameters $\zeta_m(t)$ derived from the model calculations using Eq. (4). The orange lines show the best fit ζ values (6.5 ± 1.4 and 3.7 ± 0.5 for piezo and plate, respectively). (For interpretation of the references to color in this figure legend, the reader is referred to the web version of this article.)

Likewise, we consider $\psi = 1.5$, which corresponds to the mean value found by Faug (2015) for small-scale granular flows. This parameter is kept constant, irrespective of the obstacle and sensor considered, because it represents how the mobilized volume increases with avalanche thickness. Under all these reasonable assumptions, the only free parameter is ω, which is back calculated according to piezo and plate measurements. The results are then compared to ζ values obtained as a best fit to the data, and to $\zeta(t)$.

Fig. 8, left panel, shows $\zeta(t) = p(t)/(\rho g H_{eff}(t))$ for the piezo measurements. $\zeta_m(t)$ values derived from Eq. (4) (black line) can successfully reproduce $\zeta(t)$ values (red line) by using $\omega = \omega_{piezo} = 3.55$. This is a value also used for granular flows (Faug, 2015). Predictions from Eq. (4) are not perfect but are much better than a constant ζ (orange lines in Fig. 8). In particular, the decrease of $\zeta(t)$ observed at the avalanche tail is relatively well captured by Eq. (4).

Fig. 8, right panel, shows $\zeta_m(t)$, $\zeta(t)$ and ζ for the plate measurements. Still considering $\theta = 21°$, $\rho = 400\,\mathrm{kg\,m^{-3}}$ and $\mu_e = 0.27$, we could reproduce the plate data with a value $\omega = \omega_{plate} = 3.05$. The difference between the back-calculated values of ω_{piezo} and ω_{plate} is around 15%.

To push forward the prediction of the granular model proposed by Faug (2015), one can extract the typical diameter of the mobilized volume (assumed to be cylindrical in shape), which is given by $D^* = \omega D + \psi H$. Fig. 9 displays how D^*, back-calculated with the values of ω and ψ mentioned above, would vary over time for both the pylon and the plate. The radius $D^*/2$ of the mobilized domain ranges from 2 to 4.5 m. These values confirm that the model results are physically acceptable.

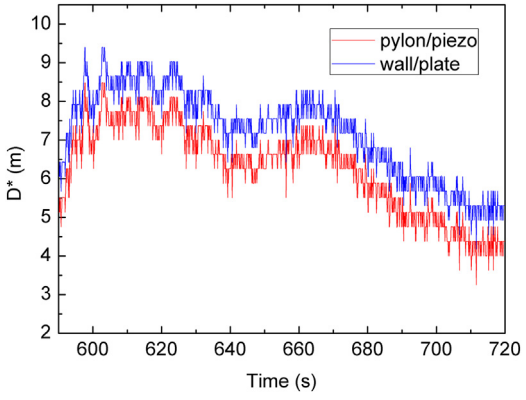

Fig. 9. Time evolution of the diameter of the mobilized volume forming upstream of the pylon (red) and wall (blue). (For interpretation of the references to color in this figure legend, the reader is referred to the web version of this article.)

6. Discussion

Almost all data analyzed in this context shows that, warm avalanches characterized by low values of Fr (typically smaller than 1), and thus under a gravitational regime condition, exert an impact pressure proportional to the flow depth, as already proposed by previous studies (Sovilla et al., 2010). The impact pressure of the only avalanche characterized by $1 \leq Fr \leq 2$, and thus in a transitional flow regime, could be reproduced successfully by adding, in addition to the depth dependent component, a velocity square component analogous to that used in granular flow studies (Faug, 2015).

However, the most striking result of our study is shown in Fig. 6, where the quasi static component of the impact pressure exerted by an avalanche on a $1\mathrm{m}^2$ plate was, on average, 1.8 times smaller that the pressure measured with the piezoelectric load cells and 2.9 time smaller than the pressure measured with the cantilever sensors, thus indicating that the avalanche-obstacle interaction is strongly controlled by the geometry of the obstacle and sensor.

Further, Fig. 6 shows that the coefficient ζ also varied between avalanches, for the same obstacle. For example, ζ coefficients measured at the plate ranged between 3.6 and 4.9. We suspect, these fluctuations were mostly associated with differences in granulometry between avalanches. As shown by Steinkogler et al. (2015), granulation regimes depend on snow temperature and liquid water content. Moist snow tends to create smaller, elasto-plastic granules (~2–10 cm in tumbler laboratory experiments) that show a quasi-brittle behavior upon impact, while wet snow generated, larger granules (~10–25 cm in the same experiments) that show a plastic behavior during impact. Thus, different dimensions and material properties have an influence on the stress distribution occurring between granules in the mobilized volume upstream of the sensor.

It is noteworthy that, the different granulation processes will change the internal friction angle of the material, ϕ, and thus have a direct influence on the definition of the model parameters, ψ and ω, that should be constant for one avalanche but clearly depend on properties of the flowing snow. For instance, the latter parameters are expected to change with grain size and shape. The grain size and

shape are controlled by friction and cohesion between snow crystals (much smaller grain scale) as well as by liquid water content. Finally, the effective basal friction, μ_e, which depends also on snow properties, may be influenced by granulometry as well.

In our back calculation, the parameters were set according to the granular experiments of Faug (2015) and topographic observations. Choosing $\psi = 1.5$ and $\mu_e = 0.27$, leads to an average $\omega = 3.3$ for avalanche #8448, which is close to the mean value of $\omega = 3$ found by Faug (2015) for idealized grains, suggesting that for this kind of avalanches the granular behavior of flowing snow prevails.

Taking into account the granular nature of the flow (Steinkogler et al., 2015), and in analogy to granular experiments, we postulate that the differences in pressure may arise from the different mobilized volume of material forming upstream of the obstacles (Faug, 2015). Fig. 9 shows that the reconstructed diameter D^* of these regions varies between 4 and 8 m for the plate and between 3.5 and 7 m for the pylon, depending on the incoming flow depth. There is not a direct measurement inside the avalanche to further demonstrate the existence of that mobilized volume or its exact geometry, but the values found for $D^*/2$ appear to be physically reasonable when they are compared to the avalanche depth (2–4 m).

Further, our analysis shows that the semi-empirical model proposed by Faug (2015) was able to reproduce the data from both the piezo and the plate by considering nearly the same set of model parameters. In particular, in our back calculation, only the parameter ω was left free. The ω difference between pylon and plate, for the same avalanche, was estimated to be about 15%. We believe that the reasons for such a discrepancy may be attributed to manifold sources. First, flow variabilities between the pylon and plate may have caused the flow depth measurements at the pylon to be less representative for the plate. Second, since the shape of the pylon and plate are different, the geometry of the mobilized volume may also differ. Finally, there may be local effects, such as the formation of a small plastic dead zone in front of the sensors and the grain size being the snow crystal, which may cause an additional increase in pressure as seen by Baroudi et al. (2011).

Indeed, an alternative framework explaining the differences in pressure exerted by wet avalanches on small load cells has been recently proposed by Baroudi et al. (2011). In their work, the mechanics of continuous media and earth passive pressure formalism is used to introduce the formation of a local wedge of snow directly on the sensor, for which the relevant grain scale is the snow crystal, which modifies the force transmission. Comparing measurements at the cantilever and piezo sensors for avalanche #8448, the impact pressure was back calculated by assuming a shear failure between moving avalanche snow and the snow wedge around the obstacle. We believe that, both approaches are relevant. Depending on the adopted formalism (continuous media mechanics with shear failure or discrete granular physics with force chains), the associated obstacle-flow volumes differ but the loadings can be accordingly reconstructed with the data. Therefore, both approaches may be investigated jointly to further improve the calculation of impact pressure on obstacles.

7. Conclusions

We analyzed impact pressures of wet avalanches, loaded under gravitational and transitional flow regimes. These pressures were measured with sensors mounted on finite-sized obstacles similar to ski or chairlift pylons. We show that the pressure exerted by wet avalanches can be reproduced accurately by a gravitational component, which, however, strongly depends on the dimensions of the obstacle and on the depth of the incoming flow. We show that the formation of a mobilized volume upstream of the obstacle can explain the measured pressures. However, verifying the existence of the mobilized volume and predicting its shape and size remains a challenge for future research on snow avalanches interacting with obstacles.

These results are of fundamental importance for the design of pylon-like structures but also for the up-scaling of impact pressure measured with small cells to larger dimensions, which are relevant for structure design. The data presented here correspond to specific geometries and dimensions and thus cannot be extrapolated to all possible geometries. While experiments conducted in full scale representing different geometries are not economically affordable, numerical simulations may help to investigate the full spectrum of geometries. An adaptation of the cohesive discrete element simulations presented by Steinkogler et al. (2015) may be a possible approach as it is capable of taking into account not only the different geometries but also the different granulometry classes and thus the important influence of snow properties.

Acknowledgments

The authors would like to thank the avalanche dynamics team and logistics staff of the WSL/SLF, the Austrian Service for Torrent and Avalanche Control - WLV, the BFW avalanche dynamics logistics team for their support in the experiments and the French ANR-Opale project. Part of this work was funded by “Canton du Valais” and by the Swiss National Foundation under grants no. 206021-113069/1 and 200021-143435. Thierry Faug is grateful for the financial support provided by the People Programme (Marie Curie Actions) of the European Unions Seventh Framework Programme under REA Grant Agreement No. 622899 (FP7-PEOPLE-2013-IOF, GRAINPACT). We gratefully thank C. Ancey and an anonymous reviewer whose suggestions helped improve and clarify this manuscript.

References

Rudolf-Miklau, F., Pfeifer, M.A., Barabási, A.-L., Schiffer, P., Rudolf-Miklau, F., 2015. The technical avalanche protection handbook. Ernst & Sohn

Albert, R., Pfeifer, M.A., Barabási, A.L., Schiffer, P., 1999. Slow drag in granular medium. Phys. Rev. Lett 82 (1), 205–208.

Ancey, C., 2006. Dynamique Des Avalanches. Presses Polytechniques et Universitaires Romandes

Ancey, C., 2015. Bain, v. Rev. Geophys

Ancey, C., Evesque, P., 2000. The frictional–collisional regime for granular suspension flows down an inclined channel. Phys. Rev. E. 62, 8349–8360.

Baroudi, D., Sovilla, B., Thibert, E., 2011. Effects of flow regime and sensor geometry on snow avalanche impact pressure measurements. J. Glaciol 57 (202), 1–12.

Dent, J.D., Burrell, K.J., Schmidt, D.S., Louge, M.Y., Adams, E., Jazbutis, T.G., 1998. Density, velocity and friction measurements in a dry snow avalanche. Ann. Glaciol 26, 247–252.

Faug, T., 2015. Macroscopic force experienced by extended objects in granular flows over a very broad Froude-number range. Eur. Phys. J. E 38 (5), 120

Forterre, Y., Pouliquen, O., 2008. Flows of dense granular media. Annu. Rev. Fluid Mech 40 (1-24),

Gauer, P., Lied, K., Kristensen, K., 2008. On avalanche measurements at the Norwegian full-scale test-site ryggfonn. Cold Reg Sci. Technol 51 (2-3), 138–155.

Jóhannesson, T., Gauer, P., Issler, D., Lied, K., 2009. The Design of Avalanche Protection Dams.

Kern, M.A., Bartelt, P., Sovilla, B., Buser, O., 2009. Measured shear rates in large dry and wet snow avalanches. J. Glaciol 55 (190), 327–338.

Kogelnig, A., Suri nach, E., Vilajosana, I., Hübl, J., Sovilla, B., Hiller, M., Dufour, F., 2011. On the complementariness of infrasound and seismic sensors for monitoring snow avalanches. Nat. Hazards Earth Syst. Sci. 11, 2355–2370.

Louge, M.Y., Steiner, R., Keast, S., Decker, R., Dent, J., Schneebeli, M., 1997. Application of capacitance instrumentation to the measurement of density and velocity of flowing snow. Cold Reg. Sci. Technol. 25 (1), 47–63.

Naaim, M., Durand, Y., Eckert, N., Chambon, G., 2013. Dense avalanche friction coefficients: influence of physical properties of snow. J. Glaciol 59 (216), 771–782.

Salm, B., 1966. Contribution to avalanche dynamics. Scientific Aspects of Snow and Ice Avalanche, Davos, IAHS Press Wallingford, Oxfordshire, UK.

Salm, B., Burkard, A., Gubler, H.U., 1990. Eidg. Institut f. Schnee- und Lawinenforschung, CH-7260 Davos Dorf.

Savage, S.B., Hutter, K., 1991. The dynamics of avalanches of granular materials from initiation to run-out. Part I. Analysis. Acta Mech. 86 (1-4), 201–223.

Schaer, M., Issler, D., 2001. Particle densities, velocities and size distribution in large avalanches from impact-sensor measurements. Ann. Glaciol 32, 321–327.

Sovilla, B., Kern, M., Schaer, M., 2010. Slow drag in wet avalanche flow. J. Glaciol 56 (198), 587–592.

Sovilla, B., McElwaine, J.N., Louge, M.Y., 2015. The structure of powder snow avalanches. C. R. Phys 16 (1), 97–104. http://dx.doi.org/10.1016/j.crhy.2014.11.005.
Sovilla, B., Schaer, M., Kern, M., Bartelt, P., 2008. Impact pressures and flow regimes in dense snow avalanches observed at the Vallée de la Sionne test site. J. Geophys. Res 113, F01010 http://dx.doi.org/10.1029/2006JF000688.
Sovilla, B., Schaer, M., Rammer, L., 2008. Measurements and analysis of full-scale avalanche impact pressure at the vallée de la Sionne test site. Cold Reg. Sci. Technol. 51, 122–137. http://dx.doi.org/10.1016/j.coldregions.2007.05.006.
Steinkogler, W., Gaume, J., Löwe, H., Sovilla, B., 2015. Lehning, m. J. Geophys. Res http://dx.doi.org/10.1002/2014JF003294.
Tiefenbacher, F., Kern, M.A., 2004. Experimental devices to determine snow avalanche basal friction and velocity profiles. Cold Reg. Sci. Technol. 38 (1), 17–30.
Tordesillas, A., Hilton, J.E., Tobin, S., 2014. Stick-slip and force chain evolution in a granular bed in response to a grain intruder. Phys. Rev. E 89, 042207.
Voellmy, A., 1955. über die zerstörungskraft von lawinen (on the destructive forces of avalanches). Schweiz. Bauztg 73 (12/15/17/19), 159–162. 212-217, 246-249, 280-285.
Vriend, N.M., McElwaine, J.N., Sovilla, B., Keylock, C.J., Ash, M., Brennan, P.V., 2013. High-resolution radar measurements of snow avalanches. Geophys. Res. Lett 40 (4), 727–731.
Wieghardt, K., 1975. Experiments in granular flow. Annu. Rev. Fluid Mech 7, 89–114.